Photocatalytic debromination enhancement of Ph-C≡C-Cu by Fe$_3$O$_4$ modification

Meng Tian [1], Ya-Ge Liu [1], Jiawei Hou, Biyun Jing, Yuanyuan Zhang, Yueru Mu, Xue Sun, Hai-Ying Jiang [*]

Key Lab of Synthetic and Natural Functional Molecule Chemistry of Ministry of Education and the Energy and Catalysis Hub, College of Chemistry and Materials Science, Northwest University, Xi'an 710127, PR China

ARTICLE INFO

ABSTRACT

A series of Fe$_3$O$_4$/Ph-C≡C-Cu magnetic hybrids were synthesized by a repeatable photothermal method in this work. The structure and morphology studies proved that Ph-C≡C-Cu grow on the surface of Fe$_3$O$_4$ in a different way, which significantly affected its physical properties and photocatalytic performance. With 4% Fe$_3$O$_4$ modification, the photocatalytic degradation rate of high concentration of pentabromophenol (PBP, 3×10^{-4} M) achieved the highest, which is 6 times higher than those of pure Ph-C≡C-Cu and Fe$_3$O$_4$. The degradation of hexabromobenzene (HBB) over Ph-C≡C-Cu was also improved to be twice higher. The excellent photocatalytic activity of Fe$_3$O$_4$/Ph-C≡C-Cu can be attributed to the big surface area, high carrier generation, transfer and separation efficiency. The TONs exceed 1 of both PBP and HBB degradation demonstrates real photocatalytic processes.

1. Introduction

Poly-halogenated chemicals (PHCs) are widely used as the flame retardant, pesticides and bactericide in our life [1–3]. However, they are also endocrine disruptors, which can lead to birth defects, tumors, cancer and other diseases, posing a threat to organisms including humans [4,5]. In the case of the increasing demand for PHCs from 1970 s, effective removal of PHCs from the environment is of great significance for human survival and health. Although PHCs can be efficiently degraded by the oxidation of Fe (VI) [6,7] and O$_3$ [8], they are generally intractable by traditionally biological and chemical oxidation processes [9–12]. Therefore, most studies focus on the reduction degradation of PHCs by strong reductants of Fe (0) [13]. In which, dehalogenations are the most important steps, and can occur in the reductive conditions. Photocatalytic technology can in situ generate strongly reducing electrons under sunlight irradiation, which can efficiently promote the dehalogenation processes, further resulting in the considerable degradation of PHCs [14–18].

Among all the previous reports, phenylacetylene copper (Ph-C≡C-Cu), a typical metal-organic coordination polymer photocatalyst, can produce electrons with the strongest reducibility of − 2.32 eV vs. SHE [19]. As we previously reported that Ph-C≡C-Cu has been proved to be favorable for the dechlorination processes in the degradation of poly-chlorinated chemicals (PCCs), such as trichloroacetic acid (TCA) [19], 2-chlorophenol (2-CP), 2,4-dichlorophenol (2,4-DCP) and 2,4, 6-trichlorophenol (2,4,6-TCP) [20]. What's more, Ph-C≡C-Cu also shows excellent performances for the reduction of toxic Cr (VI) to non-toxic Cr (III) with the modification of Ag nanoparticle [21] and UiO-66-NH$_2$ [22]. However, there are seldom reports on the degradation effect of poly-brominated chemicals (PBCs) by Ph-C≡C-Cu.

It has been reported that magnetic Fe$_3$O$_4$ shows significant effect on the debromination processes through the cycles between Fe (II) and Fe (III), and the Fe$_3$O$_4$ loading also makes photocatalysts easier to be recycled [23]. Considering these advantages, we not only studied the effect of raw Ph-C≡C-Cu for PBCs degradation, but also modified it with Fe$_3$O$_4$ nanoparticles to further enhance its activity [24–27]. Herein, Fe$_3$O$_4$/Ph-C≡C-Cu hybrids were synthesized by in situ growth of Ph-C≡C-Cu on the surface of Fe$_3$O$_4$ nanoparticles, and used for the degradation of pentabromophenol (PBP) and hexabromobenzene (HBB) under visible light irradiation. With the help of Fe$_3$O$_4$, the efficiency of Ph-C≡C-Cu in degrading PBP in 30 min was increased to be 6 times higher, which is also ~1.5 times higher than that of P25 under full

---

spectrum light irradiation. What's more, the degraded concentration of PBP in this work is 6 times higher than the highest PBP concentrations in the previous reports, resulting in the highest ratio of $m_{PBP}/m_{additive}$ of Fe$_3$O$_4$/Ph-C≡C-Cu hybrid compared to other methods. Besides, the photocatalytic degradation of HBB by Ph-C≡C-Cu was also improved by Fe$_3$O$_4$ modification with the TON of 2.15. This work developed a highly efficient and stable photocatalyst for the intractable PBCs degradations, whose efficiency exceeds the methods previously reported so far, realizing real photocatalytic reactions.

2. Experimental section

2.1. Synthesis of Fe$_3$O$_4$/Ph-C≡C-Cu

Binary magnetic Fe$_3$O$_4$/Ph-C≡C-Cu hybrids were fabricated through photothermal synthesis method [28,29]. Typically, a designed amounts of Fe$_3$O$_4$ (0 mg, 6.6 mg, 13.2 mg, 19.7 mg, 26.4 mg) and 365 mg CuCl$_2$·2 H$_2$O were added in 40 mL of methanol and stirred for 2 h, so that Fe$_3$O$_4$ and CuCl$_2$·2 H$_2$O can be mixed uniformly. Then, 1120 μL triethylamine and 440 μL phenylacetylene were successively added dropwise to the suspension under stirring, and the mixture was exposed to UV–visible light for 1 h (300 W Xe lamp, PLS-SXE300D, Beijing Perfectlight). The generated yellow-green precipitation was separated by filtering, washed with distilled water and ethanol for three times, and dried at 60 °C overnight [30]. These samples are named as x% Fe$_3$O$_4$/Ph-C≡C-Cu, where x% indicates the mass ratio of Fe$_3$O$_4$ to Ph-C≡C-Cu, which is designed to be 0, 2%, 4%, 6%, and 8%, respectively.

2.2. Photocatalytic removal evaluation

36.6 mg PBP was added to 250 mL methanol to make up 3×10^{-4} M of PBP methanol solution. 1×10^{-3} M of HBB solution was prepared by diluting 1.24×10^{-3} M of stock solution in tetrahydrofuran (THF) by methanol. All degradation reactions were carried out with irradiating the suspensions composed of pollutant solution and photocatalysts at room temperature (25 °C) by a 300 W Xenon lamp (PLS-SXE300D, Beijing Perfectlight) with a cutoff filter of $\lambda < 420$ nm. In a typical process, 5 mg of the photocatalysts and 25 mL of pollutant solution (PBP, HBB) were ultrasonically dispersed in dark for 10 min, and stirred for 20 min to reach the adsorption-desorption equilibrium. Then, argon gas was injected into the solution for 30 min to remove the air in the reactor. Afterwards, the light source was turned on and photocatalytic processes started, during which a 2 mL aliquot was sampled at every 6 min interval and centrifuged to remove photocatalysts. The samples of PBP were analyzed by high performance liquid chromatography (HPLC) with a C18 chromatographic column, and the mobile phase was 0.5% formic acid aqueous solution and methanol solution (20:80, v/v) at the flow rate of 1 mL/min, with the UV detection wavelength set at 225 nm [31]. HBB were analyzed by the HPLC analysis with a UV detector at the wavelength of 240 nm, using C-18 column, methanol (1 mL/min) as the elution solution [14]. Simultaneously, we measured the concentration of HCHO produced during the reaction by a chromogenic method. The method is as follows: 2 mL of the distilled water and 0.5 mL of the chromogenic reagent (15 g of ammonium acetate, 0.3 mL of acetic acid and 0.2 mL of acetylacetone were dissolved in 100 mL of water) were added to 0.5 mL of the liquid sample sequentially. The solution was kept for more than 1 h at 40 °C, then the concentrations of HCHO were calculated according to the standard curve by measuring the absorbances at 412 nm [32]. In addition, the degradation experiment of PBP by 4% Fe$_3$O$_4$/Ph-C≡C-Cu were also carried out at the presence of the air, 4.2 mg of AgNO$_3$ (photogenerated electrons capture), and tetrahydrofuran as solvent only, to study its photocatalytic degradation performance.

3. Results and discussion

3.1. Structure characterization

In this work, Fe$_3$O$_4$/Ph-C≡C-Cu hybrids were prepared by a repeatable photothermal method. As shown in Fig. 1, Cu^{2+} was adsorbed to Fe$_3$O$_4$ surface tightly, and then Ph-C≡C-Cu was in situ grown by light irradiation, forming Fe$_3$O$_4$/Ph-C≡C-Cu hybrids. The crystal structures of Ph-C≡C-Cu, Fe$_3$O$_4$ and Fe$_3$O$_4$/Ph-C≡C-Cu hybrids were characterized by X-ray diffraction (XRD) and exhibited in Fig. 2 A. For the XRD spectrum of Fe$_3$O$_4$, five diffraction peaks appeared at 30.10°, 35.42°, 43.05°, 56.98° and 62.57° are attributed to (220), (311), (400), (511) and (440) planes of the face centered cubic Fe$_3$O$_4$ (JCPDS no. 65–3107) [33]. For the XRD spectrum of Ph-C≡C-Cu, the three peaks at 6.0°, 9.0° and 17° are well indexed (100), (001) and (110) planes of Ph-C≡C-Cu (CCDC-242490) [29]. In comparison with pure Fe$_3$O$_4$ and Ph-C≡C-Cu, the diffraction peaks of both can be detected in the XRD pattern of Fe$_3$O$_4$/Ph-C≡C-Cu hybrids. With the increase of Fe$_3$O$_4$ content, the characteristic peak intensities of Fe$_3$O$_4$ at 35.42° and 62.57° gradually increased, while the characteristic peak of Ph-C≡C-Cu at 17° gradually decreased. This suggested that Fe$_3$O$_4$/Ph-C≡C-Cu hybrids contain both Fe$_3$O$_4$ and Ph-C≡C-Cu crystals. However, the disappearance of the peak at 6.0° belongs to Ph-C≡C-Cu in the XRD spectra of the hybrids pointed out a different growth mode of Ph-C≡C-Cu on the surface of Fe$_3$O$_4$. This phenomenon can also be observed in our previous report [28]. The optical absorbance of the as-prepared samples were also studied from UV–vis diffuse reflection spectra (UV–vis DRS) in Fig. 2B, which reveals that the light absorption band edges of the Fe$_3$O$_4$/Ph-C≡C-Cu hybrids mainly depend on that of Ph-C≡C-Cu [34,35]. This is because that Fe$_3$O$_4$ is a non-semiconductor and shows strong absorption in the whole range of UV and visible light[29,34,36,37].

The fluorescence (FL) emission spectra of the Fe$_3$O$_4$/Ph-C≡C-Cu hybrids were also performed to study the decay behavior of their photoexcited carriers. For the FL spectrum of Ph-C≡C-Cu in Fig. 2 C, the peak at 500–550 nm was assigned to the excited electrons transfer from the benzene ring to Cu, which represents the characteristic peak of electron-hole recombination for the excited Ph-C≡C-Cu [38]. It can be clearly observed that the peak intensities of the Fe$_3$O$_4$/Ph-C≡C-Cu hybrids are significantly lower than that of Ph-C≡C-Cu. Among them, the peak intensity of 4% Fe$_3$O$_4$/Ph-C≡C-Cu hybrid is the lowest, which means the lowest recombination rate and the highest separation rate of the photocarriers. This is also a beneficial factor for the photocatalytic reactions. Besides, the surface areas of the as-prepared samples, another important indicator of photocatalytic reactions, were also calculated through Brunauer-Emmett-Teller (BET) equation by the results of the Nitrogen adsorption-desorption isotherms (Fig. 2D). All the Fe$_3$O$_4$/Ph-C≡C-Cu hybrids exhibit type III isotherms corresponding to the hydrophobic surface properties of ordered organic-inorganic materials [39]. The surface areas of Fe$_3$O$_4$/Ph-C≡C-Cu hybrids are obviously larger than those of pure Ph-C≡C-Cu and Fe$_3$O$_4$. Larger surface area can provide more recombination centers, resulting to higher recombination rate of the photocarriers, which is non-profitable to the photocatalytic reaction. Therefore, the lowest recombination rate of the photocarriers was observed on 4% Fe$_3$O$_4$/Ph-C≡C-Cu hybrid with the optimal surface area of 25.7664 m^2 / g.

The morphologies and microstructures of the prepared samples were observed in scanning electron microscope (SEM) and transmission electron microscope (TEM) images. As presented in Fig. 3 A, the morphology of the pure Ph-C≡C-Cu polymer is fibrous nanoribbon-like structure and packed into bundles, while the pure Fe$_3$O$_4$ are spherical nanoparticles in Fig. 3B [40]. After the in situ growth of Ph-C≡C-Cu on the surface of Fe$_3$O$_4$, the spherical nanoparticles of Fe$_3$O$_4$ seriously agglomerated together (Fig. 3 C and D), but no fibrous structure of Ph-C≡C-Cu are observed. To further clarify the microstructure, TEM images of 4% Fe$_3$O$_4$/Ph-C≡C-Cu were acquired. It could be found in Fig. 3E that spherical Fe$_3$O$_4$ particles were indeed mixed into the fibrous

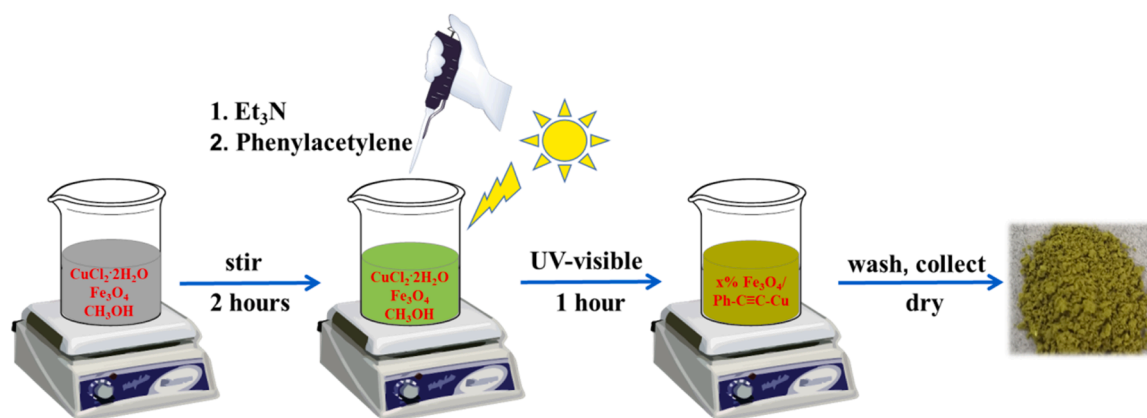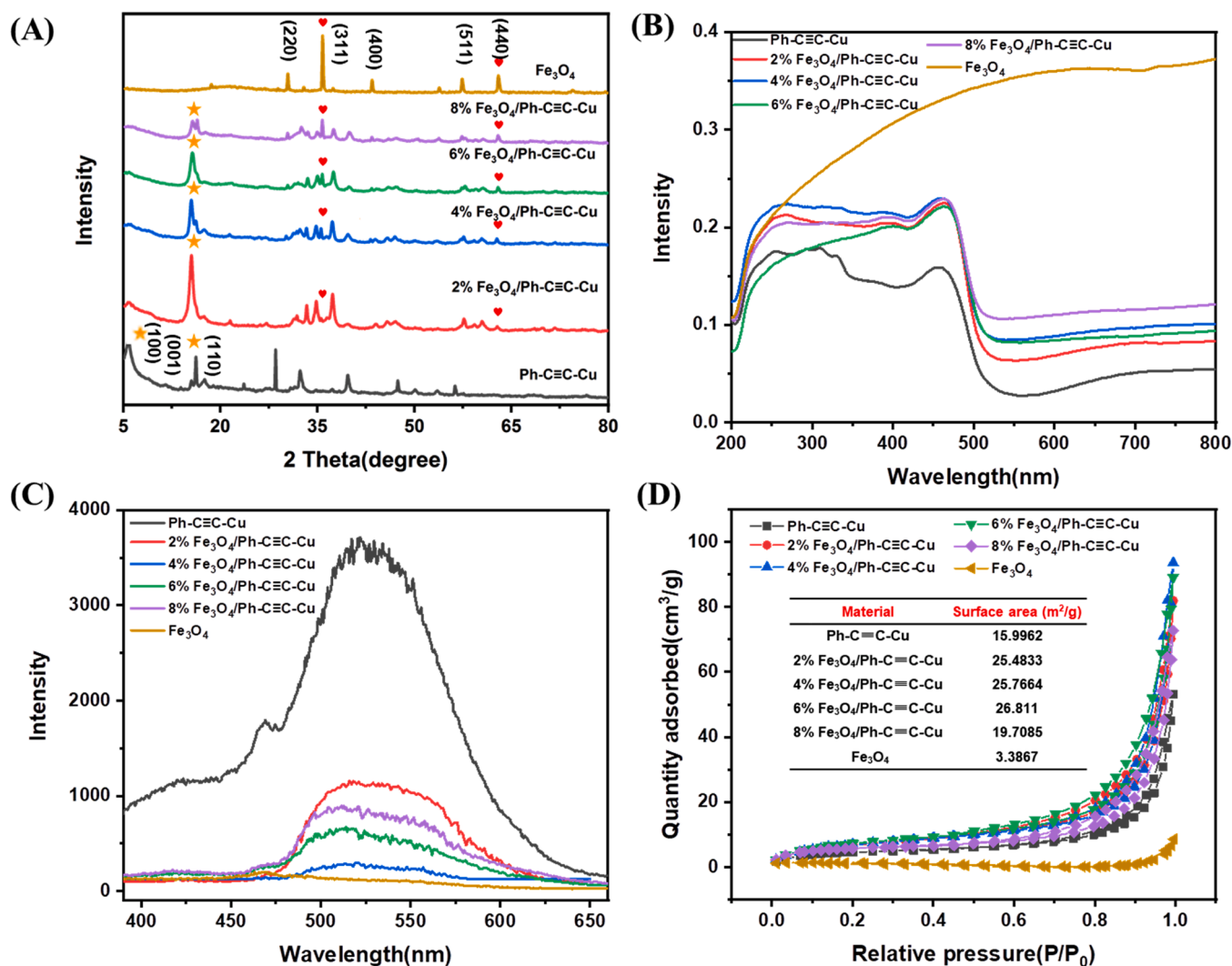**Fig. 1.** Schematic illustration of the Fe₃O₄/Ph-C≡C-Cu synthesis process.

Fig. 2. (A) XRD patterns (the marked asterisk and the heart-shaped pattern are the characteristic diffraction peaks of Ph-C≡C-Cu and Fe₃O₄, respectively), (B) UV–vis diffuse reflectance spectra, (C) Solid fluorescence spectrogram of Fe₃O₄, Ph-C≡C-Cu and *x*% Fe₃O₄/Ph-C≡C-Cu; (D) N₂ adsorption-desorption isotherms of Fe₃O₄, Ph-C≡C-Cu and *x*% Fe₃O₄/Ph-C≡C-Cu (insert shows S$_{BET}$ data).

Ph-C≡C-Cu, but the length of Ph-C≡C-Cu become much shorter. This suggests that the crystal mode and growth direction of Ph-C≡C-Cu was significantly affected by the center nucleus, being consist with the XRD results. Moreover, two sets lattice fringes with interplanar spacings of 0.593 nm and 0.389 nm (Fig. 3 F) corresponding to (771) and (533) of

cubic Fe₃O₄, confirmed that the Fe₃O₄/Ph-C≡C-Cu hybrids were successfully synthesized.

The chemical compositions and states of 4% Fe₃O₄/Ph-C≡C-Cu hybrid were confirmed by X-ray photoelectron spectroscopy (XPS). The survey spectrum of 4% Fe₃O₄/Ph-C≡C-Cu in Fig. S1 displays the peak
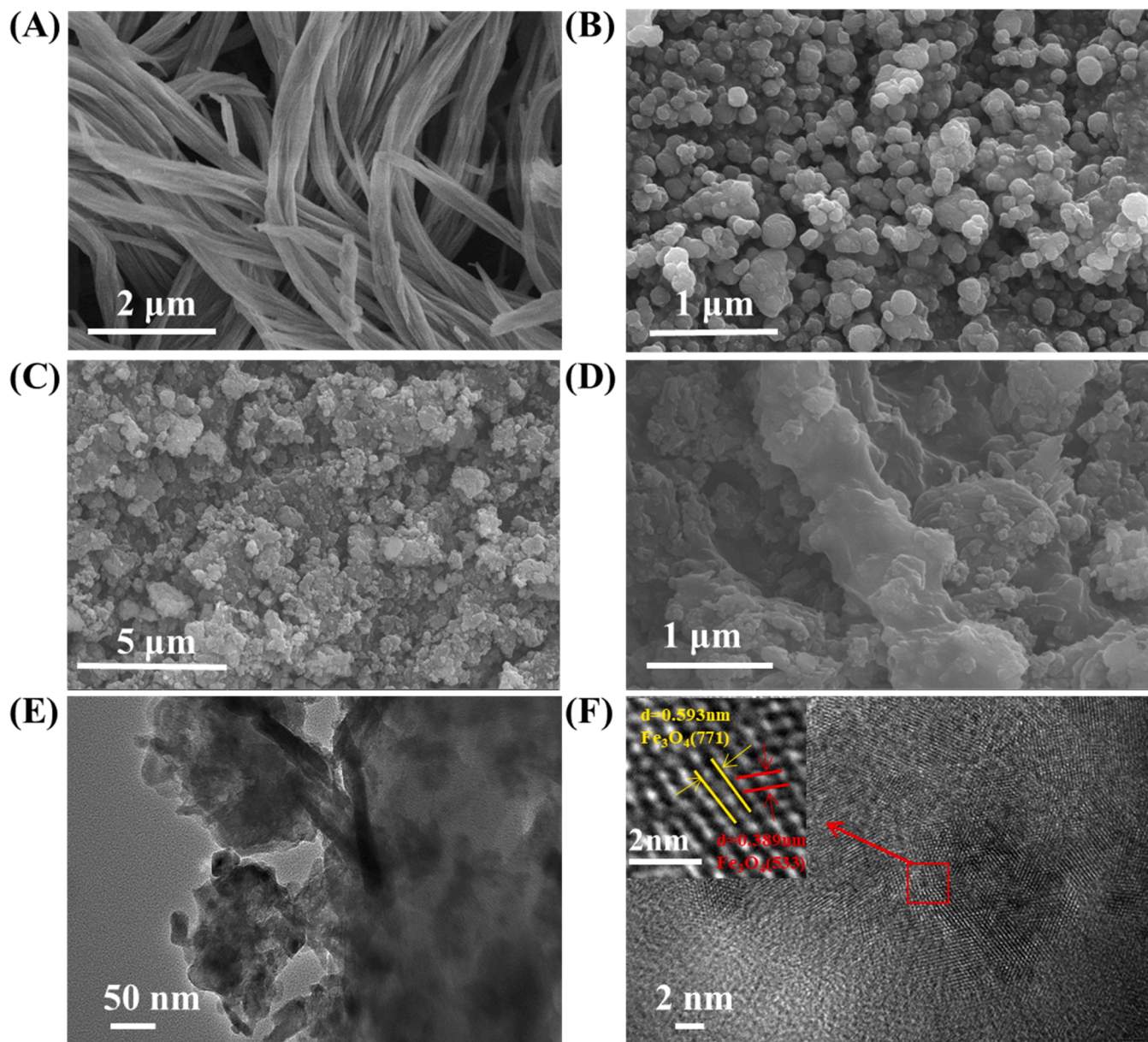
Fig. 3. (A) SEM images of Ph-C≡C-Cu sample; (B) SEM images of Fe_3O_4 sample; (C) and (D) SEM images of 4% Fe_3O_4/Ph-C≡C-Cu hybrid; (E) and (F) HRTEM of 4% Fe_3O_4/Ph-C≡C-Cu hybrid.

signatures of C, O, Fe and Cu. The high-resolution C1s peak in Fig. 4A can be divided into four peaks, which are 284.1, 284.8, 286.4, 290.4 eV, and attributed to C≡C, C=C, C=O, and COO, respectively [19]. For O 1 s, the fitted peaks at 530.2 eV and 533.2 eV (Fig. 4B) are attributed to Fe-O and COO species [19]. According to the narrow-region spectra for Fe 2p, the fitted peaks in Fig. 4C demonstrated the existence of Fe_3O_4-Fe (II)/Fe(III) NPs. These data provide the information concerning the surface of the composite and the existence of an iron-oxide layer [41–43]. The high-resolution Cu 2p spectrum (Fig. 4D) reveals that the samples contained Cu^+ and Cu^{2+} since the samples were prepared with $CuCl_2 \cdot 2 H_2O$ as the precursor of Ph-C≡C-Cu [19,44,45].

3.2. Photoelectrochemical properties

To investigate the charge generation efficiencies of the photo-catalysts, transient photocurrent responses were measured and compared. As shown in Fig. 5 A, the strong photocurrent signal indicated that pure Ph-C≡C-Cu could be photoexcited under visible-light illumination, and the negative photocurrent density suggested that Ph-C≡C-Cu is a p-type semiconductor [46]. The photocurrent density of Ph-C≡C-Cu was remarkably enhanced by Fe_3O_4 modification, especially 4% Fe_3O_4/Ph-C≡C-Cu hybrid, which shows the highest photocurrent ($\sim 3.14 \times 10^{-7}$ A), being 18 times higher than Ph-C≡C-Cu ($\sim 1.71 \times 10^{-8}$ A). The reason could be that the close interfacial contact increased the photogeneration efficiency of the excited electron-hole pairs. Moreover, the charge transfer kinetics of the samples were also investigated by electrochemical impedance spectroscopy (EIS) tests. In the Nyquist plot curves, their radiuses reflect the charge-transfer resistances at the surface of the electrode. Fig. 5B revealed that 4% Fe_3O_4/Ph-C≡C-Cu hybrid has the smallest charge transfer resistance except Fe_3O_4, because Fe_3O_4 is a good conductor.

3.3. Photocatalytic performance and mechanism

Photocatalytic performance of different samples was assessed by the photocatalytic degradation of PBP as a model pollutant in methanol. As
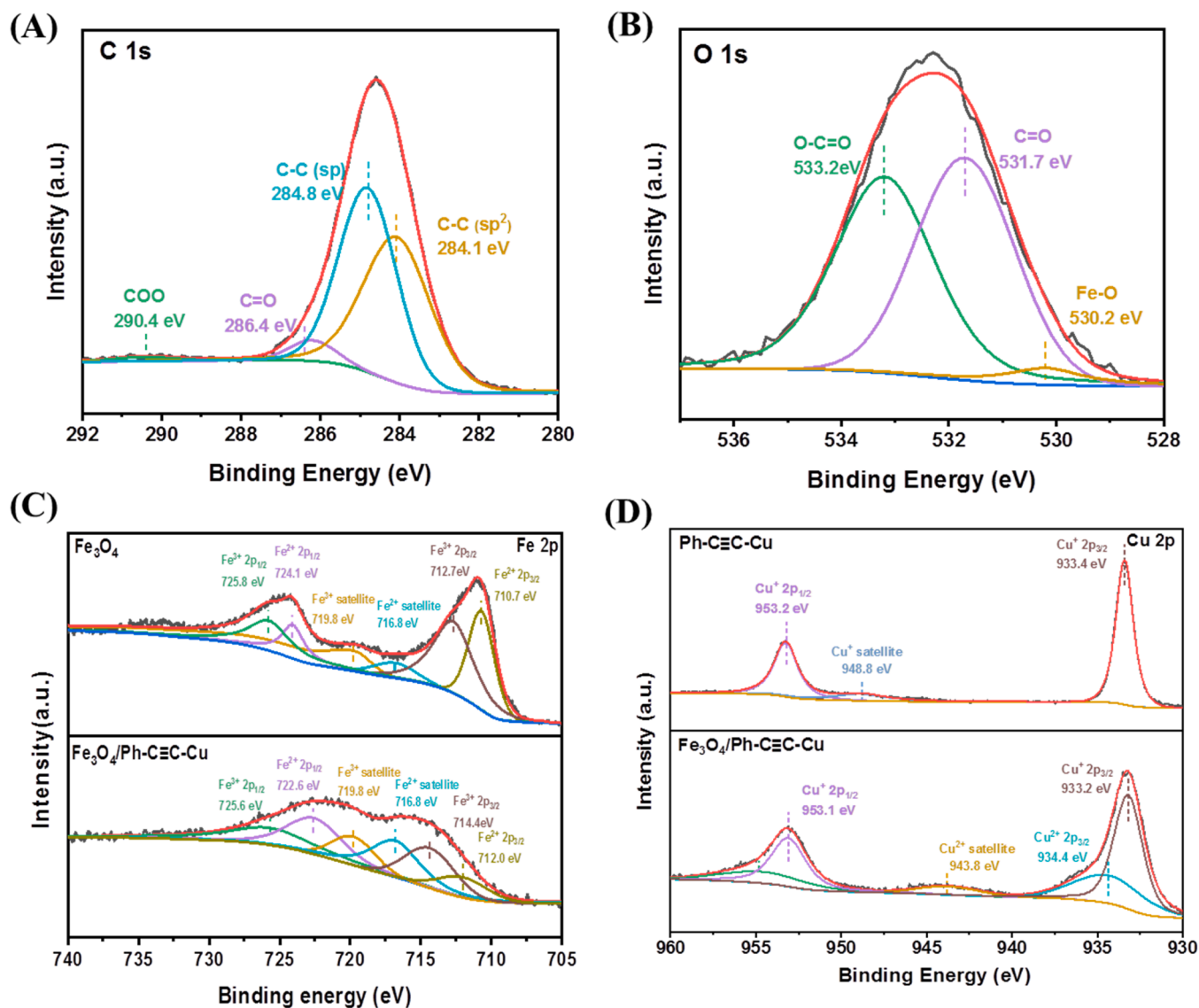
Fig. 4. X-ray photoelectron spectra of 4% Fe$_3$O$_4$/Ph-C≡C-Cu hybrid; Peak deconvolution of (A) C 1 s, (B) O 1 s, (C) Fe 2p$_{1/2}$ & Fe 2p$_{3/2}$, (D) Cu 2p$_{1/2}$ & Cu 2p$_{3/2}$. All deconvoluted peaks are assigned with its chemical bonds.

illustrated in Fig. 6 A, PBP cannot be degraded by only either photocatalyst in dark or single light without photocatalyst. Meanwhile, less than 20% of the PBP can be photocatalytic degraded by both pure Fe$_3$O$_4$ and Ph-C≡C-Cu. When they are combined together, the photocatalytic degradation efficiency of PBP is significantly improved, even exceeding the efficiency of P25. As the characterization results, 4% Fe$_3$O$_4$/Ph-C≡C-Cu shows the biggest surface area, the highest photocurrent density, the lowest FL intensity and the smallest charge-transfer resistance, hence it also shows the highest degradation efficiency of PBP. The degradation rate of PBP in 30 min by 4% Fe$_3$O$_4$/Ph-C≡C-Cu achieved 94.35%, which is 6 times higher than that of single Fe$_3$O$_4$ or Ph-C≡C-Cu, and 1.5 times higher than that of the commercial P25. The recycling experiments clearly show that no significant decrease of photocatalytic efficiency was observed after 5 recycling tests, suggesting a good stability and recyclability of 4% Fe$_3$O$_4$/Ph-C≡C-Cu hybrid.

The photocatalytic products of PBP degradation by 4% Fe$_3$O$_4$/Ph-C≡C-Cu hybrid were further tested and measured. Bromides were taken off gradually and produced phenol at last (Fig. S2A). The produced phenol by Ph-C≡C-Cu and 4% Fe$_3$O$_4$/Ph-C≡C-Cu were quantitatively measured and displayed in Fig. S2B and C, respectively. The production rate of phenol by Fe$_3$O$_4$/Ph-C≡C-Cu hybrid is also faster than that by Ph-

C≡C-Cu. After 3 h irradiation, all the bromides were taken off by Fe$_3$O$_4$/Ph-C≡C-Cu, being accompanied by the absolute transformation of PBP to phenol, which can be easily degraded by the traditional oxidation methods. This result suggests its excellent debromination effect. In order to clarify whether the debromination processes occurred through oxidation or reduction effect, the PBP were also degraded in air. The results in Fig. 6 C show that the photocatalytic degradation of PBP was obviously depressed by the O$_2$ in air, pointing out the dominant reducing effect on debromination process. It was speculated that O$_2$ will completely react with photoexcited electrons to generate reactive oxygen species (ROS), weakening the reductive debromination processes. Moreover, the degradation of PBP was almost absolutely depressed when we added AgNO$_3$ as the electron capture (Fig. 6D). At the same time of reducing debromination by the conduction band electrons, some solvent of CH$_3$OH were oxidized to HCHO (Fig. S2D) by the valence band hole, and these two half-reactions form an overall reaction. The oxidation of CH$_3$OH is also very important for the degradation of PBP, which can be seriously inhibited by the absence of CH$_3$OH. The same to the generation of phenol, 4% Fe$_3$O$_4$/Ph-C≡C-Cu hybrid also produced more HCHO than Ph-C≡C-Cu. The apparent quantum yields (AQY) of the photocatalytic PBP degradation over the prepared 4% Fe$_3$O$_4$/Ph-
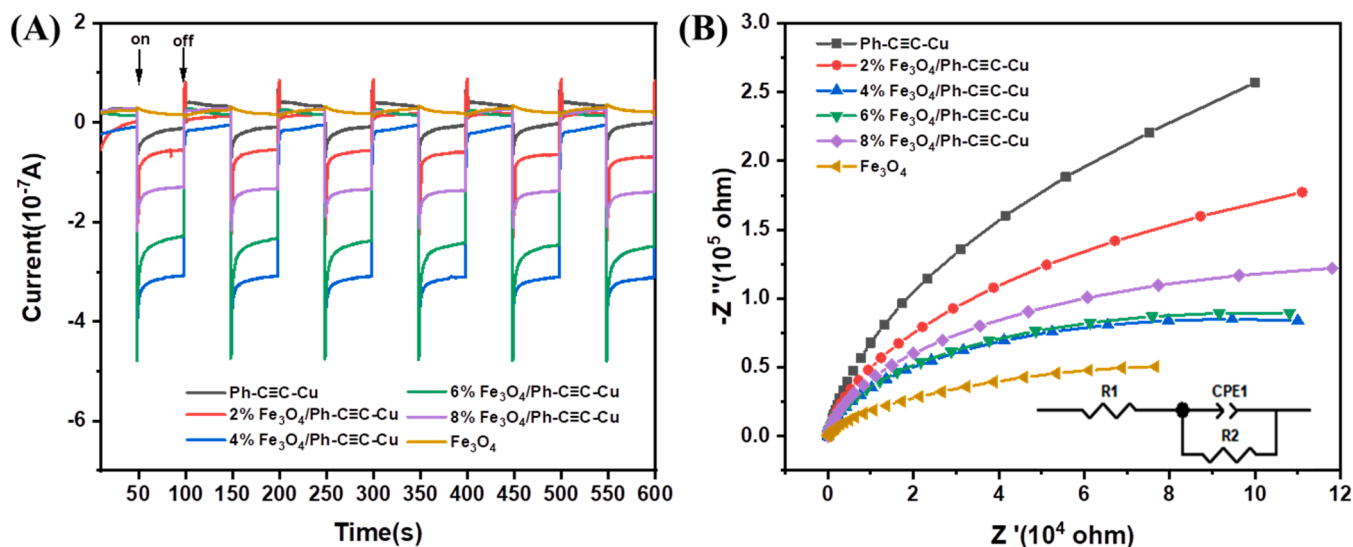
Fig. 5. (A) Time dependent photocurrent curves of the as-prepared Fe$_3$O$_4$/Ph-C≡C-Cu hybrids; (B) Electrochemical impedance spectroscopy of the as-prepared Fe$_3$O$_4$/Ph-C≡C-Cu hybrids; Inset: the equivalent circuit.

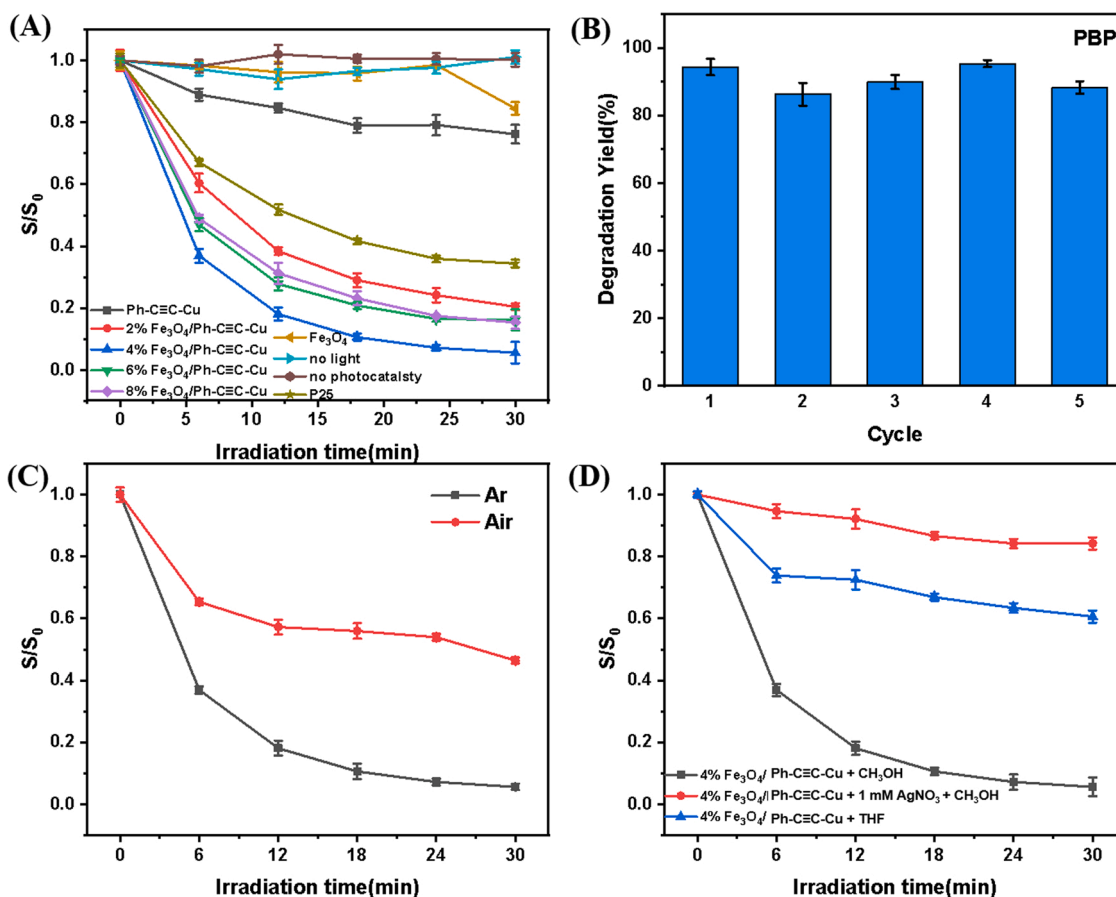**Fig. 6.** (A) Photocatalytic degradation of PBP over the Fe$_3$O$_4$/Ph-C≡C-Cu hybrids under different conditions under; (B) Cycling experiments of PBP degradation over the 4% Fe$_3$O$_4$/Ph-C≡C-Cu hybrid; Photocatalytic degradation of PBP over the 4% Fe$_3$O$_4$/Ph-C≡C-Cu hybrid in air and Ar, respectively; (D) Photocatalytic degradation of PBP over the 4% Fe$_3$O$_4$/Ph-C≡C-Cu hybrid under different conditions. Light Source: 300 W Xenon lamp (PLS-SXE300D, Beijing Perfectlight), P25：Full spectrum; Other materials：λ > 420 nm

C≡C-Cu t were also measured under the homogeneous light at wavelengths 420 and 500 nm. They are 0.18% for the light of 420 nm and 0.06% for the light of 500 nm, respectively (Fig. S3, Supporting Information).

Being compared with the previous reports on PBP degradation by other methods (Table 1), both the concentration of PBP and the total $m_{Pollutant}/m_{additive}$ in this work are the highest, showing the absolute predominance. The total turnover number (TON) of 4% Fe$_3$O$_4$/Ph-C≡C-

Table 1
Summary of PBP degradation from different literature works.

Additive	C_{PBP} (mol/L)	$C_{additive}$	Solvent	Light source	Irradiation/degradation time	Degradation rate	TON[a]	$m_{PBP}/m_{additive}$	Ref.
Fe(VI)	2×10^{-5}	0.4 mM	H_2O	-	5 min	100%	0.050	0.12	[6]
O_3	5×10^{-5}	-	phosphate buffer	-	5 min	100%	-	-	[8]
FeTPyP-SBA-15	5×10^{-5}	0.1 g/L	-	-	30 min	95%	21.74	0.23	[31]
0.16%Cu/TiO$_2$	1×10^{-5}	0.2 g/L	THF	300 W Xe lamp ($\lambda > 360$ nm)	25 min	75%	3×10^{-3}	0.018	[14]
4% Fe$_3$O$_4$/ Ph-C≡C-Cu	3×10^{-4}	0.2 g/L	methanol	300 W Xe lamp ($\lambda > 420$ nm)	30 min	95%	1.22[b]	3.63[b]	This work

[a] TON $= n_{PBP}/n_{additive}$;
[b] 5 cycles.

Cu hybrid for 5 cycles PBP degradation experiment was calculated as 1.22, indicating that this is a non-equivalent reaction, but a real catalytic reaction.

Photocatalytic generation of ROS was measured to further evaluate the promotion effect of Fe$_3$O$_4$ modification for photocatalytic performance of Fe$_3$O$_4$/Ph-C≡C-Cu. The $\cdot O_2$ and H_2O_2 concentrations generated by the photocatalytic reaction of 4% Fe$_3$O$_4$/Ph-C≡C-Cu sample were both higher than those of pure Ph-C≡C-Cu in Fig. S4A and S4B. Semi-quatitative generation of ·OH shows that its formation over 4% Fe$_3$O$_4$/Ph-C≡C-Cu (Fig. S4C) was faster and higher than that over Ph-C≡C-Cu (Fig. S4D). These phenomenons indicate that 4% Fe$_3$O$_4$/Ph-C≡C-Cu hybrid can produce more conduction band electrons.

Based on the results and discussions above, the plausible mechanism of photocatalytic degradation of PBP by Fe$_3$O$_4$/Ph-C≡C-Cu hybrids is proposed as shown in Fig. 7. Ph-C≡C-Cu is excited to generate excited electron-hole pairs under visible light irradiation. On the one hand, the formed conduction band electrons of Ph-C≡C-Cu can transfer to Fe$_3$O$_4$, to reduce Fe^{3+} to Fe^{2+} (E (Fe^{3+}/ Fe^{2+}) = 0.77 V vs. SHE) [23], because of their strong reducing ability (−2.32 V vs. SHE) [19]. As reported, the in situ formed Fe^{2+} can reduce PBP to debrominate and generate phenol. At the same time, Fe^{2+} recovered to Fe^{3+}. Then, the produced phenol can be further degraded into non-toxic inorganic small molecules by the traditional oxidation technology [47,48]. On the other hand, Cu$^+$ in Ph-C≡C-Cu becomes Cu^{2+} when the valence electrons are excited to its conduction band. The in situ formed Cu^{2+} oxidizes CH$_3$OH to HCHO and restors Cu$^+$ by itself. In general, Fe$_3$O$_4$ can be served as electron trapping centers to restrain the fast recombination of photo-generated carriers

through the interconversion between Fe^{3+} and Fe^{2+}, while methanol can be served as hole trapping centers. Moreover, since the reduction of PBP to phenol requires five electrons and the oxidation of methanol to formaldehyde consumes only two holes, the stoichiometric ratio of phenol to formaldehyde is 2:5, being consist with the results in Fig. S2C and D. Fe$_3$O$_4$/Ph-C≡C-Cu hybrids exhibits much higher photocatalytic performance than single Ph-C≡C-Cu and Fe$_3$O$_4$, and their outstanding photocatalytic performances are attributed to the synergistic effect of optimal surface area, high generation and higher separation of photocarriers.

After the photocatalytic degradation reaction, the XPS of the 4% Fe$_3$O$_4$/Ph-C≡C-Cu were characterized and displayed in Fig. 8. The valence states of both Fe and Cu didn't change during the photocatalytic degradation of PBP, which again proves good stability of 4% Fe$_3$O$_4$/Ph-C≡C-Cu. According to our previous report [19], the conversion of Cu$^+$ to Cu^{2+} was observed during the photocatalytic reactions, which is attributed to the excitation of valence electrons from Cu$^+$. Fortunately, the formed Cu^{2+} during the photocatalytic reaction can be recovered to Cu$^+$ by the addition of sacrificial agent, like reductive ascorbic acid. In this system, the decreased content of Cu^{2+} after photocatalytic degradation, based on the results of XPS spectra before and after photo-catalytic reaction (Fig. 8B), suggests the recovering of Cu^{2+} to Cu$^+$ by the sacrificial agent of reductive CH$_3$OH and prove the mechanism we propose in Fig. 7. However, the conversion between Fe^{2+} and Fe^{3+} is dynamically changing and very difficult to monitor their valence states.

After speculating a rational photocatalytic mechanism, we continued to study the photocatalytic degradation performance of Fe$_3$O$_4$/Ph-C≡C-
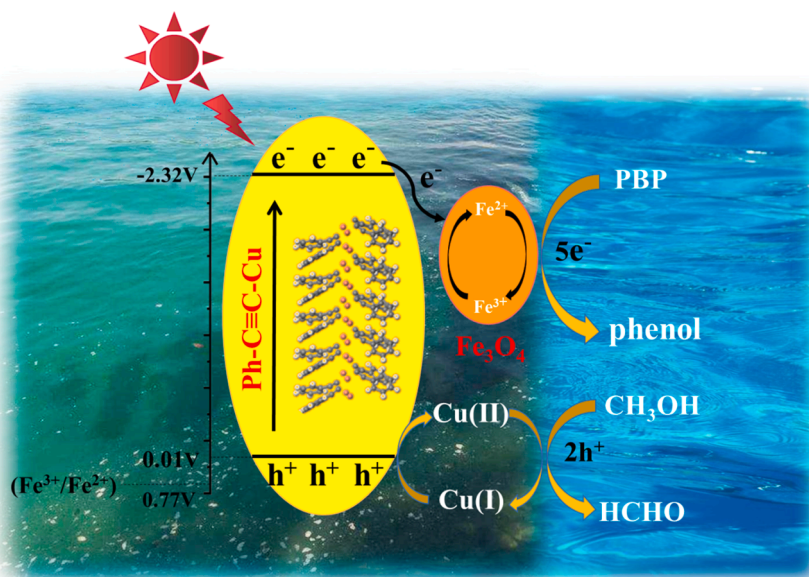
Fig. 7. Illustration of the potential photocatalytic mechanism of the Fe$_3$O$_4$/Ph-C≡C-Cu system.
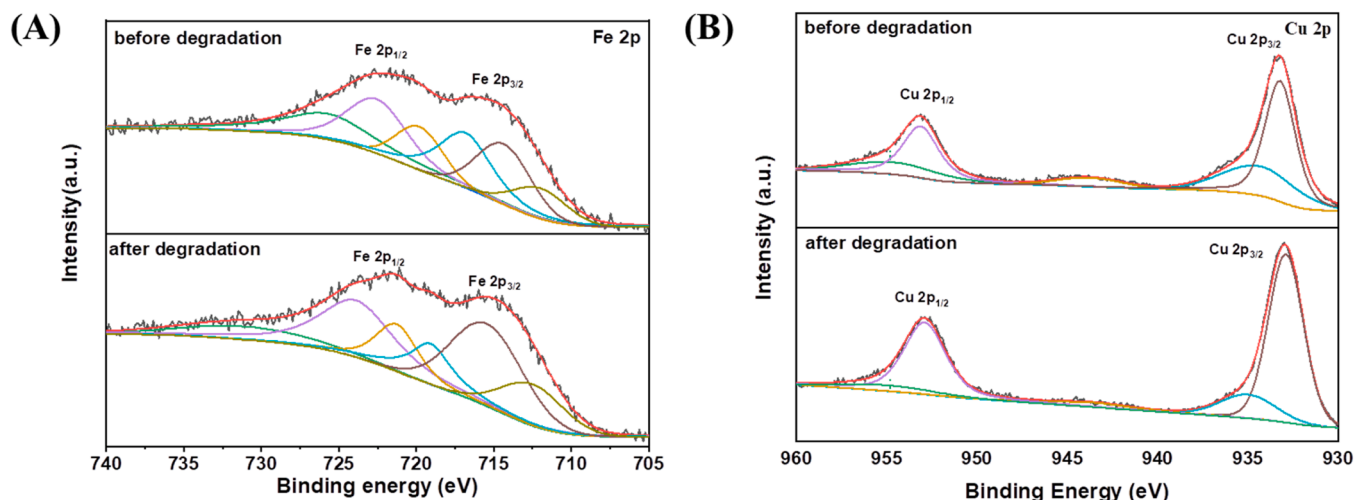
Fig. 8. The comparison of X-ray photoelectron spectra of 4% Fe$_3$O$_4$/Ph-C≡C-Cu hybrid between before and after the photodegradation reaction; (A) Fe 2p$_{1/2}$ & Fe 2p$_{3/2}$, (B) Cu 2p$_{1/2}$ & Cu 2p$_{3/2}$. All deconvoluted peaks are assigned with its chemical bonds.

Cu hybrids to other brominated aromatic hydrocarbons. Fig. 9 A shows the temporal evolution of visible spectrum of HBB solution photo-catalyzed by 4% Fe$_3$O$_4$/Ph-C≡C-Cu at room temperature. The degra-dation rate of HBB reached 83.64% after 30 min' irradiation, which is about twice higher than that by pure Ph-C≡C-Cu (45.92%). The degradation rate of HBB over 4% Fe$_3$O$_4$/Ph-C≡C-Cu sample was kept above 80% in the first three cycling experiments, but the degradation rate began to decrease in the fourth cycle. For the 8th cycle, it decreased to 39.96% (Fig. 9B). In total, the TON of 8 cycles HBB degradation was determined to be 2.15, which demonstrated that this is a real catalytic reaction again. The sharp decrease of the photocatalytic activity from the 4th cycle was attributed to the degraded products accumulation on the surface of Fe$_3$O$_4$/Ph-C≡C-Cu magnetic hybrids, which will be further degraded in the later experiments firstly. After that, the newly supple-mented PBP in the solution can be degraded.

4. Conclusion

In summary, this work successfully constructed Fe$_3$O$_4$ modified Ph-C≡C-Cu magnetic hybrids for efficiently debromination processes. The XRD, SEM and TEM spectra demonstrated a different crystal mode and growth direction of Ph-C≡C-Cu on the surface of Fe$_3$O$_4$, which are beneficial to increase the surface area of Ph-C≡C-Cu, enhancing the generation of photocarriers, promoting the charge transfer and separa-tion. As a result, the photocatalytic degradation of both PBP and HBB over Ph-C≡C-Cu are significantly improved. The highest photocatalytic degradation rate in 30 min of PBP achieved on 4% Fe$_3$O$_4$/Ph-C≡C-Cu hybrid, which reached 94.35%, being 6 times higher than those by bare Ph-C≡C-Cu and Fe$_3$O$_4$. The photocatalytic degradation rate of HBB over Ph-C≡C-Cu was also improved to twice higher by Fe$_3$O$_4$ modification. Most importantly, the TON numbers of both PBP and HBB exceed 1, realizing real photocatalytic reactions.

CRediT authorship contribution statement

Meng Tian: Writing – original draft. **Ya-Ge Liu:** Methodology, Data curation, Writing – review & editing. **Jiawei Hou:** Formal analysis, Data curation. **Biyun Jing:** Data curation. **Yuanyuan Zhang:** Investigation. **Yueru Mu:** Data curation. **Xue Sun:** Data curation. **Hai-Ying Jiang:** Supervision, Conceptualization, Writing – review & editing, Funding acquisition.
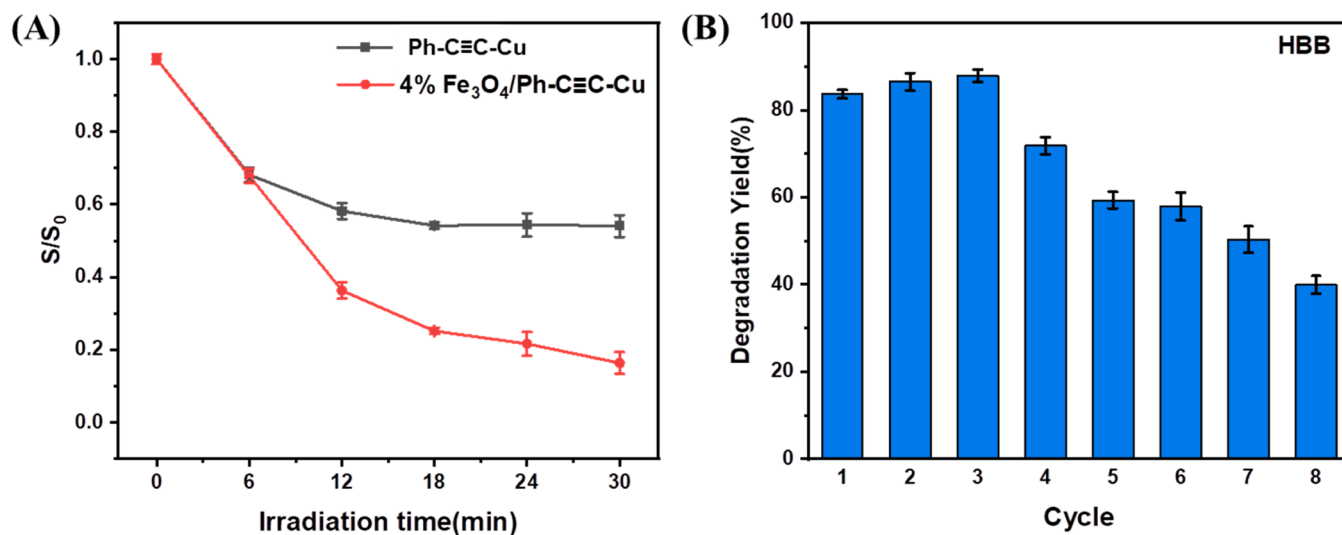

Fig. 9. (A) Photocatalytic degradation of HBB over the Ph-C≡C-Cu and 4% Fe$_3$O$_4$/Ph-C≡C-Cu hybrid; (B) Cycling experiments of HBB degradation over the 4% Fe$_3$O$_4$/Ph-C≡C-Cu hybrid.

Declaration of Competing Interest

The authors declare that they have no known competing financial interests or personal relationships that could have appeared to influence the work reported in this paper.

Data Availability

Data will be made available on request.

Acknowledgement

Appendix A. Supporting information

Supplementary data associated with this article can be found in the online version at doi:10.1016/j.apcatb.2023.122866.

References

[1] H. Mizukawa, K. Nomiyama, S. Nakatsu, M. Yamamoto, M. Ishizuka, Y. Ikenaka, S. M.M. Nakayama, S. Tanabe, Anthropogenic and naturally produced brominated phenols in pet blood and pet food in Japan, Environ. Sci. Technol. 51 (2017) 11354–11362, https://doi.org/10.1021/acs.est.7b01009.

[2] Y. Wang, G. Jiang, P.K.S. Lam, A. Li, Polybrominated diphenyl ether in the East Asian environment: A critical review, Environ. Int. 33 (2007) 963–973, https://doi.org/10.1016/j.envint.2007.03.016.

[3] G. Yu, Q. Bu, Z. Cao, X. Du, J. Xia, M. Wu, J. Huang, Brominated flame retardants (BFRs): A review on environmental contamination in China, Chemosphere 150 (2016) 479–490, https://doi.org/10.1016/j.chemosphere.2015.12.034.

[4] C.S. Rosenfeld, N.D. Denslow, E.F. Orlando, J.M. Gutierrez-Villagomez, V. L. Trudeau, Neuroendocrine disruption of organizational and activational hormone programming in poikilothermic vertebrates, J. Toxicol. Environ. Health B Crit. Rev. 20 (2017) 276–304, https://doi.org/10.1080/10937404.2017.1370083.

[5] R. Dallaire, E. Dewailly, D. Pereg, S. Dery, P. Ayotte, Thyroid function and plasma concentrations of polyhalogenated compounds in Inuit adults, Environ. Health Perspect. 117 (2009) 1380–1386, https://doi.org/10.1289/ehp.0900633.

[6] A.A. Dar, J. Chen, A. Shad, X. Pan, J. Yao, M. Bin-Jumah, A.A. Allam, Z. Huo, F. Zhu, Z. Wang, A combined experimental and computational study on the oxidative degradation of bromophenols by Fe(VI) and the formation of self-coupling products, Environ. Pollut. 258 (2020), 113678, https://doi.org/10.1016/j.envpol.2019.113678.

[7] Y. Fei, Z. Liu, L. Meng, G. Liu, D. Kong, X. Pan, F. Zhu, J. Lu, J. Chen, Experimental and theoretical study on Fe(VI) oxidative degradation of dichlorophen in water: kinetics and reaction mechanisms, Environ. Pollut. 306 (2022) 119394, https://doi.org/10.1016/j.envpol.2022.119394.

[8] A.A. Dar, X. Wang, S. Wang, J. Ge, A. Shad, F. Ai, Z. Wang, Ozonation of pentabromophenol in aqueous basic medium: kinetics, pathways, mechanism, dimerization and toxicity assessment, Chemosphere 220 (2019) 546–555, https://doi.org/10.1016/j.chemosphere.2018.12.154.

[9] D. Chen, J. Shen, X. Jiang, G. Su, W. Han, X. Sun, J. Li, Y. Mu, L. Wang, Simultaneous debromination and mineralization of bromophenol in an up-flow electricity-stimulated anaerobic system, Water Res. 157 (2019) 8–18, https://doi.org/10.1016/j.watres.2019.03.054.

[10] M. Dopico, A. Gomez, Review of the current state and main sources of dioxins around the world, J. Air Waste Manag. Assoc. 65 (2015) 1033–1049, https://doi.org/10.1080/10962247.2015.1058869.

[11] R. Golan, F. Gelman, T. Kuder, A.A. Taylor, Z. Ronen, A. Bernstein, Degradation of 4-bromophenol by Ochrobactrum sp. HI1 isolated from desert soil: pathway and isotope effects, Biodegradation 30 (2019) 37–46, https://doi.org/10.1007/s10532-018-9860-y.

[12] Q. Zhang, Y. Liu, Y. Lin, W. Kong, X. Zhao, T. Ruan, J. Liu, J.L. Schnoor, G. Jiang, Multiple metabolic pathways of 2,4,6-tribromophenol in rice plants, Environ. Sci. Technol. 53 (2019) 7473–7482, https://doi.org/10.1021/acs.est.9b01514.

[13] X. Wu, S. Lu, Z. Qiu, Q. Sui, K. Lin, X. Du, Q. Luo, The reductive degradation of 1,1,1-trichloroethane by Fe(0) in a soil slurry system, Environ. Sci. Pollut. Res. 21 (2014) 1401–1410, https://doi.org/10.1007/s11356-013-2029-7.

[14] Y. Lv, X. Cao, H. Jiang, W. Song, C. Chen, J. Zhao, Rapid photocatalytic debromination on TiO2 with in-situ formed copper co-catalyst: Enhanced adsorption and visible light activity, Appl. Catal. B 194 (2016) 150–156, https://doi.org/10.1016/j.apcatb.2016.04.053.

[15] J. Xiao, Y. Xie, H. Cao, Organic pollutants removal in wastewater by heterogeneous photocatalytic ozonation, Chemosphere 121 (2015) 1–17, https://doi.org/10.1016/j.chemosphere.2014.10.072.

[16] M. Yang, T. Xu, M. Jin, Q. Shen, C. Sun, Oxygen vacancies enriched Bi2WO6 for enhanced decabromodiphenyl ether photodegradation via C-Br bond activation, Appl. Surf. Sci. 581 (2022), 152439, https://doi.org/10.1016/j.apsusc.2022.152439.

[17] T. Xu, M. Yang, C. Chen, R. Duan, Q. Shen, C. Sun, Photocatalytic activation of C-Br bond on facet-dependent BiOCl with oxygen vacancies, Appl. Surf. Sci. 548 (2021), 149243, https://doi.org/10.1016/j.apsusc.2021.149243.

[18] G. Sheng, Y. Shao, W. Ye, C. Sun, C. Chen, J.C. Crittenden, C. Liu, Weak-bond-based photoreduction of polybrominated diphenyl ethers on graphene in water, ACS Sustain Chem. Eng. 6 (2018) 6711–6717, https://doi.org/10.1021/acssuschemeng.8b00494.

[19] H.-Y. Jiang, P. Zhou, Y. Wang, R. Duan, C. Chen, W. Song, J. Zhao, Copper-based coordination polymer nanostructure for visible light photocatalysis, Adv. Mater. 28 (2016) 9776–9781, https://doi.org/10.1002/adma.201603556.

[20] M. Tian, J. Qian, J. Hou, Y. Bai, H.-Y. Jiang, J. Ren, Promotion effect of free Ag$^+$ ions on photocatalytic dechlorination processes, Catal. Sci. Technol. 12 (2022) 3209–3218, https://doi.org/10.1039/D1CY02210E.

[21] X. Jin, Y. Wu, Z. Lin, D. Liang, F. Wang, X. Zheng, H. Liu, W. Lv, G. Liu, Plasmonic Ag nanoparticles decorated copper-phenylacetylide polymer for visible-light-driven photocatalytic reduction of Cr(VI) and degradation of PPCPs: Performance, kinetics, and mechanism, J. Hazard. Mater. 425 (2022), 127599, https://doi.org/10.1016/j.jhazmat.2021.127599.

[22] Z. Lin, Y. Wu, X. Jin, D. Liang, Y. Jin, S. Huang, Z. Wang, H. Liu, P. Chen, W. Lv, G. Liu, Facile synthesis of direct Z-scheme UiO-66-NH2/PhC2Cu heterojunction with ultrahigh redox potential for enhanced photocatalytic Cr(VI) reduction and NOR degradation, J. Hazard Mater. 443 (2023), 130195, https://doi.org/10.1016/j.jhazmat.2022.130195.

[23] Y. Wang, J. Gao, Y. Liu, M. Li, M. Zhang, G. He, Z. Sun, Facile fabrication of ZnO nanorods modified Fe3O4 nanoparticles with enhanced magnetic, photoelectrochemical and photocatalytic properties, Opt. Mater. 111 (2021), 110608, https://doi.org/10.1016/j.optmat.2020.110608.

[24] H.T. Bui, S.M. Im, K.-J. Kim, W. Kim, H. Lee, Photocatalytic degradation of phenolic compounds of defect engineered Fe3O4: an alternative approach to solar activation via ligand-to-metal charge transfer, Appl. Surf. Sci. 509 (2020), 144853, https://doi.org/10.1016/j.apsusc.2019.144853.

[25] R. Santhosh Kumar, K. Govindan, S. Ramakrishnan, A.R. Kim, J.-S. Kim, D.J. Yoo, Fe3O4 nanorods decorated on polypyrrole/reduced graphene oxide for electrochemical detection of dopamine and photocatalytic degradation of acetaminophen, Appl. Surf. Sci. 556 (2021), 149765, https://doi.org/10.1016/j.apsusc.2021.149765.

[26] S. Xuan, W. Jiang, X. Gong, Y. Hu, Z. Chen, Magnetically separable Fe3O4/TiO2 hollow spheres: fabrication and photocatalytic activity, J. Phys. Chem. C 113 (2009) 553–558, https://doi.org/10.1021/jp8073859.

[27] X. Zhao, Z. Lu, M. Wei, M. Zhang, H. Dong, C. Yi, R. Ji, Y. Yan, Synergetic effect of carbon sphere derived from yeast with magnetism and cobalt oxide nanochains towards improving photodegradation activity for various pollutants, Appl. Catal. B. 220 (2018) 137–147, https://doi.org/10.1016/j.apcatb.2017.08.037.

[28] H.-Y. Jiang, J. Qian, J. Hou, M. Tian, Y. Bai, C. Li, High concentration of methyl orange elimination by targeted construction of an α-Bi2O3/Ph-C-C-Cu Z-scheme, Catal. Sci. Technol. 12 (2022) 7122–7132, https://doi.org/10.1039/D2CY01590K.

[29] J. Qian, W. Dang, J. Li, W. Zhang, M. Tian, N. Wang, W. Song, L. Lv, H.-Y. Jiang, Photo(electro)catalytic activity enhancement of PhC2Cu by Fe doping induced energy band modulation and luminescence chromism switching, Catal. Sci. Technol. 11 (2021) 2379–2385, https://doi.org/10.1039/D0CY02355H.

[30] X. Xie, Y. Qiu, S. Zhao, H.-Y. Jiang, J. Lu, Photo-synthesized copper phenylacetylide nanobelts with preferential photocatalytic active facet exposure, Korean J. Chem. Eng. 35 (2018) 2127–2132, https://doi.org/10.1007/s11814-018-0121-x.

[31] Q. Zhu, S. Maeno, R. Nishimoto, T. Miyamoto, M. Fukushima, Oxidative degradation of pentabromophenol in the presence of humic substances catalyzed by a SBA-15 supported iron-porphyrin catalyst, J. Mol. Catal. A: Chem. 385 (2014) 31–37, https://doi.org/10.1016/j.molcata.2014.01.013.

[32] H. Song, X. Meng, S. Wang, W. Zhou, X. Wang, T. Kako, J. Ye, Direct and selective photocatalytic oxidation of CH4 to oxygenates with O2 on cocatalysts/ZnO at room temperature in water, J. Am. Chem. Soc. 141 (2019) 20507–20515, https://doi.org/10.1021/jacs.9b11440.

[33] Q. Zhang, L. Yu, C. Xu, W. Zhang, M. Chen, Q. Xu, G. Diao, A novel method for facile preparation of recoverable Fe3O4@TiO2 core-shell nanospheres and their advanced photocatalytic application, Chem. Phys. Lett. 761 (2020), 138073, https://doi.org/10.1016/j.cplett.2020.138073.

[34] T. Wang, S. Zhong, S. Zou, F. Jiang, L. Feng, X. Su, Novel Bi2WO6-coupled Fe3O4 magnetic photocatalysts: preparation, characterization and photodegradation of tetracycline hydrochloride, Photochem. Photobiol. 93 (2017) 1034–1042, https://doi.org/10.1111/php.12739.

[35] Y. Chen, X. Jin, Preparation of Fe3O4@SiO2@BiO1.8·0.04H2O/Ag3PO4 magnetic nanocomposite and its photocatalytic performance, Ceram. Int. 45 (2019) 1283–1292, https://doi.org/10.1016/j.ceramint.2018.10.012.

[36] E.A. Volnistem, R.D. Bini, D.M. Silva, J.M. Rosso, G.S. Dias, L.F. Cótica, I.A. Santos, Intensifying the photocatalytic degradation of methylene blue by the formation of BiFeO3/Fe3O4 nanointerfaces, Ceram. Int. 46 (2020) 18768–18777, https://doi.org/10.1016/j.ceramint.2020.04.194.

[37] M. Xiao, R. Li, J. Yin, J. Yang, X. Hu, H. Xiao, W. Wang, T. Yang, Enhanced photocatalytic oxidation of As(III) by TiO2 modified with Fe3O4 through Ti-O-Fe

interface bonds, Colloids Surf. 651 (2022), 129678, https://doi.org/10.1016/j.colsurfa.2022.129678.

[38] S.S.Y. Chui, M.F.Y. Ng, C.-M. Che, Structure determination of homoleptic Au[I], Ag[I], and Cu[I] Aryl/alkylethynyl coordination polymers by X-ray powder diffraction, Chem. Eur. J. 11 (2005) 1739–1749, https://doi.org/10.1002/chem.200400881.

[39] M. Kruk, M. Jaroniec, Gas adsorption characterization of ordered organic−inorganic nanocomposite materials, Chem. Mater. 13 (2001) 3169–3183, https://doi.org/10.1021/cm0101069.

[40] F. Chang, H. Chen, X. Zhang, B. Lei, X. Hu, N-p heterojunction $Bi_4O_5I_2/Fe_3O_4$ composites with efficiently magnetic recyclability and enhanced visible-light-driven photocatalytic performance, Sep. Purif. Technol. 238 (2020), 116442, https://doi.org/10.1016/j.seppur.2019.116442.

[41] S.H. Yoo, D. Jang, H.-I. Joh, S. Lee, Iron oxide/porous carbon as a heterogeneous Fenton catalyst for fast decomposition of hydrogen peroxide and efficient removal of methylene blue, J. Mater. 5 (2017) 748–755, https://doi.org/10.1039/c6ta07457j.

[42] X. Lv, W. Prastistho, Q. Yang, C. Tokoro, Application of nano-scale zero-valent iron adsorbed on magnetite nanoparticles for removal of carbon tetrachloride: Products and degradation pathway, Appl. Organomet Chem. 34 (2020), e5592, https://doi.org/10.1002/aoc.5592.

[43] M. Xiao, R. Li, X. Hu, W. Zhu, Z. Yu, H. Xiao, W. Wang, T. Yang, Construction of in-situ carbon-doped TiO_2 decorated Fe_3O_4 heterojunction and their enhanced

photocatalytic oxidation of As(III) under visible light, Sep. Purif. 300 (2022), 121836, https://doi.org/10.1016/j.seppur.2022.121836.

[44] S. Guan, G.E. Rossi, J.M. Winfield, C. Wilson, D. MacLaren, D.J. Morgan, P. R. Davies, D.J. Willock, D. Lennon, The interaction of CO with a copper((II)) chloride oxy-chlorination catalyst, Faraday Discuss. 229 (2021) 318–340, https://doi.org/10.1039/d0fd00014k.

[45] S.Y. Lee, N. Mettlach, N. Nguyen, Y.M. Sun, J.M. White, Copper oxide reduction through vacuum annealing, Appl. Surf. Sci. 206 (2003) 102–109, https://doi.org/10.1016/S0169-4332(02)01239-4.

[46] Z. Wei, J. Hu, K. Zhu, W. Wei, X. Ma, Y. Zhu, Self-assembled polymer phenylethnylcopper nanowires for photoelectrochemical and photocatalytic performance under visible light, Appl. Catal. B. 226 (2018) 616–623, https://doi.org/10.1016/j.apcatb.2017.12.070.

[47] R. Wang, L. Du, W. Gao, J. Li, N.T. Tsona, X. Zhang, X. Hu, W. Wang, H. Liu, Enhanced photocatalytic performance of PdO-loaded heterostructured nanobelts to degrade phenol, Chemosphere 276 (2021), 130266, https://doi.org/10.1016/j.chemosphere.2021.130266.

[48] C. Feng, Z. Chen, J. Jing, J. Hou, The photocatalytic phenol degradation mechanism of Ag-modified ZnO nanorods, J. Mater. Chem. C 8 (2020) 3000–3009, https://doi.org/10.1039/C9TC05010H.